Correlating Substrate Reactivity at Electrified Interfaces with the Electrolyte Structure in Synthetically Relevant Organic Solvent/Water Mixtures

Florian Dorchies, Alessandra Serva, Astrid Sidos, Laurent Michot, Michaël Deschamps, Mathieu Salanne, Alexis Grimaud

Correlating substrates reactivity at electrified interfaces with electrolyte structure in synthetically relevant organic solvent/water mixtures

Florian Dorchies[1,2], Alessandra Serva[2,3], Astrid Sidos[4,5], Laurent Michot[3], Michaël Deschamps[2,6], Mathieu Salanne[2,3,7], and Alexis Grimaud[1,2,4]*

[1] Chimie du Solide et de l'Energie, UMR 8260, Collège de France, 75231 Paris Cedex 05, France

[2] Réseau sur le stockage Electrochimique de l'Energie (RS2E), CNRS FR3459, 80039 Amiens Cedex, France

[3] Sorbonne Université, CNRS, Physicochimie des Électrolytes et Nanosystèmes Interfaciaux, PHENIX, F-75005 Paris, France

[4] Department of Chemistry, Merkert Chemistry Center, Boston College, Chestnut Hill, Massachusetts 02467, United States

[5] Chemistry Department, École Normale Supérieure, PSL University, 75005 Paris, France

[6] CNRS, CEMHTI, UPR 3079, Université d'Orléans, F-45071 Orléans, France

[7] Institut Universitaire de France (IUF), 75231 Paris, France

*Correspondence to alexis.grimaud@bc.edu

ABSTRACT

Optimizing electrosynthetic reactions requires fine tuning of a vast chemical space, including charge transfer at electrocatalyst/electrode surfaces, engineering of mass transport limitations and complex interactions of reactants and products with their environment. Hybrid electrolytes, in which supporting salt ions and substrates are dissolved in a binary mixture of organic solvent and water, represent a new piece to this complex puzzle, as they offer a unique opportunity to harness water as the oxygen or proton source in electrosynthesis. In this work, we demonstrate that modulating water-organic solvent interactions drastically impacts the solvation properties of hybrid electrolytes. Combining various spectroscopies with synchrotron small-angle X-ray scattering (SAXS) and force field-based molecular dynamics (MD) simulations, we show that the size and composition of aqueous domains forming in hybrid electrolytes can be controlled. We demonstrate that water is more reactive for the hydrogen evolution reaction (HER) in aqueous domains than when strongly interacting with solvent molecules, which originates from a change in reaction kinetics rather than from a thermodynamic effect. We exemplify novel opportunities arising from this new knowledge for optimizing electrosynthetic reactions in hybrid electrolytes. For reactions proceeding first *via* the activation of water, fine tuning of aqueous domains impacts the kinetics and potentially the selectivity of the reaction. Instead, for organic substrates reacting prior to water, aqueous domains have no impact on reaction kinetics, while selectivity may be affected. We believe that such fine comprehension of solvation properties of hybrid electrolytes can be transposed to numerous electrosynthetic reactions.

INTRODUCTION

The field of electrocatalysis has long been driven by the design of ever better electrocatalysts with optimal adsorption energy for reaction intermediates, allowing to steer selectivity and kinetics of various reactions. Nevertheless, the past few years have seen a growing interest being paid to the role of non-covalent interactions in liquid electrolytes and at electrochemical interfaces, with numerous demonstrations of their role in governing the outcome of electrocatalytic and electrosynthetic reactions.[1–3] Hence, both the kinetics and selectivity of aqueous electrocatalytic reactions have been tuned by electrolyte engineering approaches, in particular through the use of tailored supporting salt ions. Pivotal results were obtained for the hydrogen evolution reaction (HER),[4,5] the oxygen evolution reaction (OER)[6,7] and the CO_2 and N_2 reduction reactions.[8–11] This strategy was also successfully adopted for electrosynthetic reactions in aqueous electrolytes, including to control the competition between the HER and the electrohydrodimerization of acrylonitrile.[12,13] In organic electrosynthesis, beyond the nature of supporting salt ions, the solvent itself can impact the selectivity. For instance, the solvent deprotonation free energy controls the selectivity (carboxylation *vs* hydrogenolysis) in organic halide electrocarboxylation.[14] Instead, the solvent coordinating power was shown to control the yield of the anodic fluorination of 4-arylthio-1,3-dioxolan-2-ones through the (de)stabilization of the radical cation intermediate.[15]

In the quest towards greener reactants, mixtures of organic solvent and water with a supporting salt (denoted as "hybrid electrolytes") are currently investigated to harness water either as the oxygen-atom source in anodic reactions[16–24] or as the proton/deuterium source in electrochemical protonation/deuteration of alkyl, aryl and benzylic halides[23,25–27] and alkynes.[23,26] These mixtures constitute a novel class of electrolytes and offer a formidable playground to tune electrocatalytic and electrosynthetic reactions *via* the modulation of the electrolyte nano/microstructure.[1] Indeed,

while binary mixtures of water and water-soluble organic solvents are macroscopically homogeneous, bulk heterogeneity can occur at different length scales depending on the molar fraction of water and the nature of the organic solvent. When establishing strong hydrogen bonds, the organic solvent molecules and water can mix at the molecular scale, as postulated for dimethylformamide(DMF)/water mixtures.[28–31] On the contrary, when water and the organic solvent only weakly interact, such as for ACN/water mixtures, two types of domains are co-existing at the nanoscale, one rich in organic solvent molecules and one aqueous.[32–36]

Although extensive research has been conducted on binary organic solvent/water mixtures, little is known regarding their local structure in presence of supporting salts, with the exception of ACN/water mixtures.[16,32,37,38] The size of the aqueous domains depends on the molar fraction of water and the concentration of supporting salt, with volumes for the aqueous domains found in the range of 200 – 1000 $Å^3$ as computed by molecular dynamics (MD) simulations.[32] Such domains are conserved at the electrochemical interface and large aqueous domains were found to correlate with an increased reactivity of water towards the HER,[32] as a result of better diffusion properties of hydroxyls and hydronium ions. Furthermore, the hydrophilicity of the electrochemical interface was shown to be tuned by the nature of the supporting salt cation in ACN/water mixtures.[16,38] We recently exploited this feature to steer the yield of the epoxidation of cyclooctene at gold electrodes.[16]

Hence, state of the art research in this field is limited to tuning the size of aqueous domains by modulating water concentration and Lewis acidity of salt cations, while the role of organic solvent/water interactions has remained elusive. Without this fundamental piece, the generality of this strategy to modulate the reactivity of aqueous heterogeneities for electrocatalytic and electrosynthetic applications is yet to be demonstrated. Equally important for the application,

beyond tuning non-covalent interactions and water dynamics, hybrid electrolytes were shown to induce a shift in redox reactions, including the HER.[32,38] Nevertheless, the origin for such shift remains uncertain. Indeed, as previously observed for other non-ideal/diluted electrolytes, such shift in potential could be kinetic, and thus be harvested to reduce the cell potential by improving one half reaction, or simply arise from a shift in thermodynamic potential, which would shift both half-reactions in the same manner and thus provide zero gain in energy for the overall process.

In this work, we investigate how the solvation properties of hybrid organic solvent/water electrolytes can impact the electrochemical reactivity of water and the outcome of electrosynthetic reactions. Toward that goal, four binary mixtures were selected, using DMF, ACN, tetrahydrofuran (THF) and acetone as organic solvents. Among these mixtures, DMF and water form strong hydrogen bonds, leading to little to no microheterogeneity. Instead, ACN and water are shown to weakly interact, leading to the formation of aqueous and organic nanodomains. Acetone and THF, for which the binary mixtures with water were also shown to exhibit heterogeneity at the nanoscale,[39–48] interact stronger with water than ACN does *via* the formation of hydrogen bonds with their oxygen atom. By combining NMR and IR spectroscopy, synchrotron small-angle X-ray scattering (SAXS) and force field-based MD simulations of the four bulk mixtures, we first investigate in details their structures at short and intermediate range. Our results demonstrate that organic solvents can be used to tune aqueous heterogeneities in hybrid electrolytes and that the water structure in the different mixtures modulates its reactivity at electrified interfaces. By comparing these results with those collected from two recently developed electrosynthetic reactions, namely the electrochemical oxidation of sulfides[20,24] and the electrochemical deuteration of benzylic halides,[27] we demonstrate that the effect of aqueous heterogeneities in organic electrolytes depends on the mechanism. Looking into the effect of electrolyte structuration, we

provide quantitative analysis of the impact of solvation structure on the kinetics of reactions. Overall, our study answers critical questions regarding the effect of the short to intermediate range structure in synthetically relevant organic solvent/water mixtures.

RESULTS AND DISCUSSION

Characterization of the mixtures.

For each mixture, the concentration of water is set at 5.0 M, a concentration previously shown to result in optimal Faradaic efficiency of reactions such as the epoxidation of alkenes, while maintaining sufficient solubility for the organic substrates.[16,17,19] Unless stated otherwise, the mixtures contain 0.1 M $LiClO_4$ as supporting salt. In the mixtures of ACN, acetone, DMF and THF with 5.0 M water and 0.1 M $LiClO_4$, the molar fraction of water is equal to 0.222, 0.283, 0.294 and 0.305, respectively, as determined by experimentally measuring their densities (Tables S1-4). The excess enthalpy of mixing (ΔH^{mix}) of the mixtures provides a good indication of the strength of the solvent-water interactions (hydrogen bonding being the dominating one), with negative (positive) values indicating stronger (weaker) solvent-water interactions than solvent-solvent and water-water interactions. On the whole composition range, ΔH^{mix} was reported to be positive for ACN/water (except at molar fractions of water greater than 0.97)[49] and negative for DMF/water[50] while it is positive for acetone/water[51] and THF/water[52] for a molar fraction of water below 0.4 (Figure S1). DMF and water molecules form stronger hydrogen bonds than those between water molecules whereas hydrogen bonds formed between ACN, acetone, THF and water molecules are weaker. This difference in strength can be observed qualitatively by looking at the attenuated total reflection (ATR) IR spectra of the mixtures (Figure 1a and Figure S2 for the mixtures without supporting salt), with the wavenumber of the O-H stretching mode of water

evolving in the order ACN < acetone < DMF ≈ THF and the intensity evolving in the order ACN < acetone ≈ THF < DMF. The observed trend for the O-H stretching mode of water suggests that in the mixtures, the hydrogen bonds formed between water and ACN are the weakest and the strongest with DMF, while acetone and THF constitute intermediate cases.[53] However, the bands are large and the ATR intensity depends on the difference between the refractive index of the ATR prism and the liquid, thus making quantitative interpretation of the O-H stretching mode of water difficult (see discussion below Figure S2). Unfortunately, no insights can be gained from the bending mode of water, which is also a powerful probe of the hydrogen-bonding network,[54] due to its overlap with solvent bands in the 1500 – 1800 cm^{-1} region (Figure S3).

Besides O-H stretching vibrations, the ^{1}H NMR chemical shift of water is also strongly affected by the nature of the solvent in the mixture (Figure 1b). While the presence of $LiClO_4$ causes a downfield shift of ^{1}H $\delta(H_2O)$ due to the strong Li^{+}-OH_2 interactions,[32] the observed trend between the different mixtures remains unaffected by the salt (Figures S4 and S5). The establishment of hydrogen bonds with an electronegative acceptor atom such as oxygen or nitrogen is correlated to a downfield shift of the hydrogen-bonded hydrogen nucleus.[55] The ^{1}H NMR chemical shift of water in the ACN mixture appears at more upfield chemical shifts than in the other mixtures (Figure 1b). Nevertheless, we refrain from drawing quantitative conclusions from the ^{1}H NMR results regarding the strength of hydrogen bonding between the different organic solvent/water systems. Indeed, the chemical shift of a nucleus is related to its electron density and, aside from the formation of hydrogen bonds, it can be influenced by the electron density of the acceptor atom, i.e., the organic solvent here (see discussion in Figure S6).

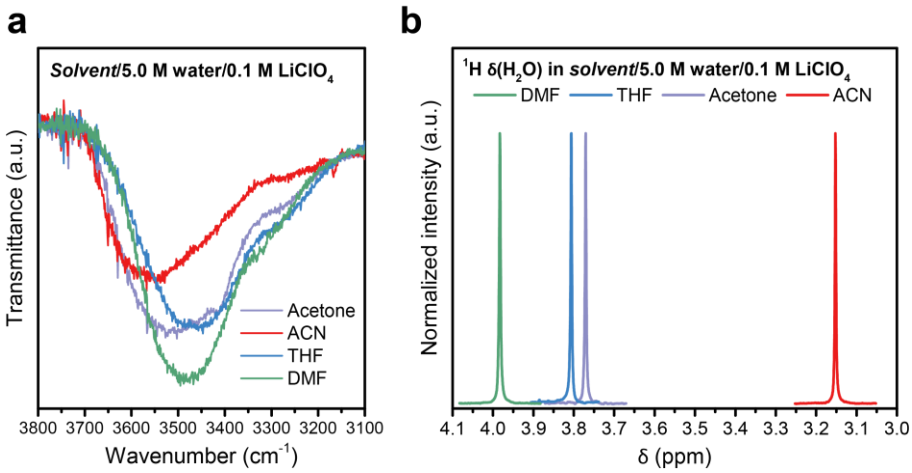

Figure 1. (a) ATR IR spectra in the 3800 – 3100 cm^{-1} region and (b) normalized ^{1}H NMR peaks of water in solvent/5.0 M water/0.1 M $LiClO_4$ mixtures. Tetramethylsilane (TMS) is used as an internal reference and is set at 0.00 ppm.

To obtain more direct evidence of the extent of microheterogeneity, we turned to synchrotron small-angle X-ray scattering (SAXS), a technique sensitive to nanoscale electron density variation previously successfully implemented to reveal the solvation structure of various electrolytes for electrocatalytic and battery applications.[37,56] The presence of $LiClO_4$ in the mixtures increases the experimentally measured SAXS intensity due to the presence of Cl atoms, which have a higher atomic number than the atoms in the solvent and water molecules and thus scatter more X-rays (Figures S7-14). To overcome this issue and solely probe aqueous heterogeneities, the SAXS patterns of solvent/0.1 M $LiClO_4$ and solvent/5.0 M water/0.1 M $LiClO_4$ mixtures were measured (Figure 2a,b) and subtracted in the 0.02 to 0.6 $Å^{-1}$ q range (Figure 2c). This is the q range of interest for studying local heterogeneities in the electrolytes, which corresponds to distances of 10.4 to 314.2 Å ($2\pi/q$).[56] Strikingly, the SAXS pattern of DMF/5.0 M water/0.1 M $LiClO_4$ is relatively flat in the 0.02 to 0.6 $Å^{-1}$ q range and no increase in SAXS intensity is observed compared to DMF/0.1 M $LiClO_4$ containing no water. On the contrary, the SAXS patterns of the three other

solvent/5.0 M water/0.1 M $LiClO_4$ mixtures have a characteristic shape[37,56] showing a marked increase in intensity compared to the patterns of the water-free solvent/0.1 M $LiClO_4$ mixtures. This marked distinction between DMF on the one hand and ACN, THF and acetone on the other hand is also observed without supporting salt (Figure S15). The SAXS results confirm that, as previously postulated, little to no heterogeneity is evidenced at the nanoscale in DMF/5.0 M water mixtures because of the formation of strong DMF-water hydrogen bonds. Conversely, heterogeneities form at the nanoscale in mixtures of ACN, THF and acetone with 5.0 M water. One can note that a few simulation[57,58] and experimental studies[59,60] report some degree of heterogeneity in DMF/water mixtures, especially around equimolar ratios. These results will be discussed below in light of our MD simulations.

The SAXS intensity depends on the electronic contrast, i.e., the average difference in scattering length density (combined sum of the scattering lengths of the atoms – SLD) between aqueous and organic regions in these mixtures.[61] At 16 keV, the energy at which the SAXS experiments were performed, the SLD (in 10^{-6} $Å^{-2}$) of water, DMF, THF, acetone and ACN are equal to 9.433, 8.774, 8.385, 7.337 and 7.154, respectively.[62] Among all solvents, the electronic contrast between water and DMF is the lowest. However, the SLD of THF is close to that of DMF (and in THF/5.0 M water, the molar fraction of water is very close to that in DMF/5.0 M water) while its mixture with water gives rise to the highest SAXS intensity (Figure 2c). Therefore, even though the smaller electronic contrast between DMF and water certainly plays a role in the low SAXS intensity obtained for DMF/5.0 M water mixtures, the different SAXS patterns cannot be simply explained by different electronic contrasts. To grasp further insights into the nanoscale heterogeneities in the different mixtures, in particular their size and shape, and confirm our interpretation of the SAXS results, force field-based MD simulations were performed.

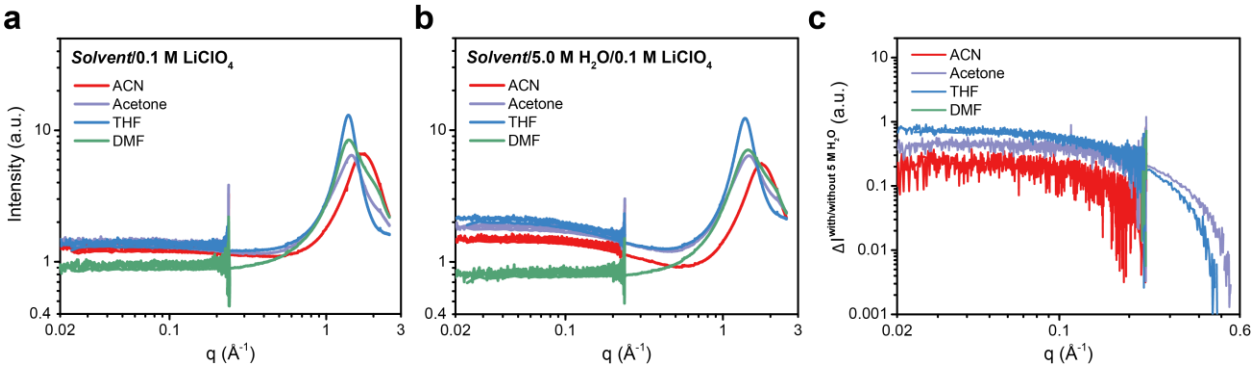

Figure 2. Synchrotron SAXS patterns of (a) solvent/0.1 M $LiClO_4$ and (b) solvent/5.0 M water/0.1 M $LiClO_4$ mixtures in the 0.02 to 3.0 $Å^{-1}$ q range. (c) Difference in intensity between the SAXS patterns of solvent/5.0 M water/0.1 M $LiClO_4$ and solvent/0.1 M $LiClO_4$ mixtures in the 0.02 to 0.6 $Å^{-1}$ q range. For each pattern, the discontinuity at 0.238 $Å^{-1}$ corresponds to the change from the small to the wide angle configuration of the setup, corresponding to sample-to-detector distances of 6.2 m and 0.5 m, respectively. For each pattern, the two curves are plotted as obtained experimentally. They are superimposable, hence showing the good quality of the measurement. In the 0.02 to 0.6 $Å^{-1}$ q range, the intensity of the DMF/5.0 M water/0.1 M $LiClO_4$ pattern is either equal or slightly lower than that of DMF/0.1 M $LiClO_4$, indicating that the subtraction cannot be observed in log-log scale on panel c.

First, it is worth noting that the results of force field-based MD simulations strongly depend on the chosen force fields. We thus tested several force fields for the solvents to reproduce as best as possible the experimental SAXS patterns, i.e., the short to intermediate range structure in the mixtures (see Supplementary Information 1 and Experimental Section). For each system, the composition of the box was determined by experimentally measuring the density of the corresponding mixture. Large ~ 100 * 100 * 100 $Å^3$ (Tables S1-4) boxes were used to simulate SAXS patterns at low q while maintaining reasonable computational times. For such box sizes, the lowest accessible value of q is equal to $2\pi/100 = 0.0628$ $Å^{-1}$, which is also the resolution of the calculation. Aqueous nanodomains (in red) are visible on the snapshots of the simulations of the mixtures with ACN, acetone and THF while water molecules are homogeneously distributed in the mixture with DMF (Figure 3a-d). For each system, SAXS patterns were calculated from the MD simulations with the GROMACS utilities (see Experimental Section and Supplementary Information 1 for details). Very good agreement between the experimental and the simulated

SAXS patterns is obtained (Figure 3e-h), showing that our simulations accurately reproduce the structure of the mixtures. We note that a slight discrepancy exists between the experimental and the simulated SAXS patterns for the DMF-based mixture (Figure 3h), which we discuss in details in Supplementary Information 1.

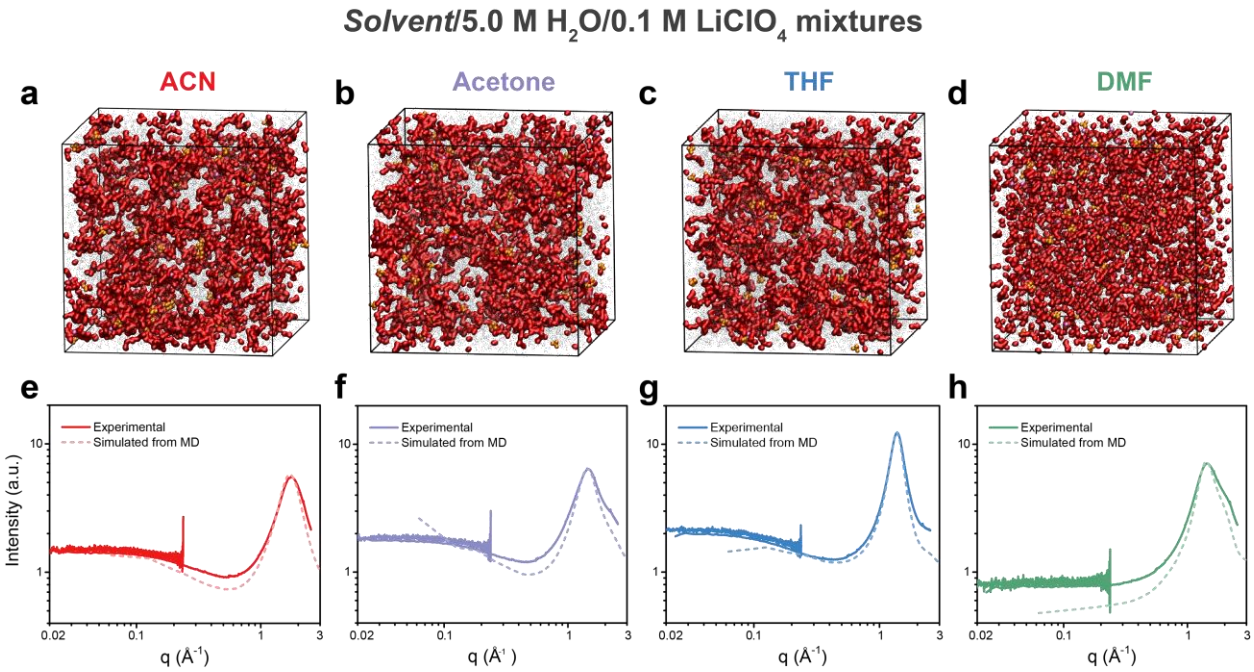

Figure 3. Snapshots of the MD simulations of the solvent/5.0 M H_2O/0.1 M $LiClO_4$ mixtures with (a) ACN, (b) acetone, (c) THF and (d) DMF. Water molecules are represented in red, Li^+ in mauve, ClO_4^- in orange and solvent molecules in gray (the size of which are decreased for clarity). In panels e-h are plotted the corresponding experimental and simulated SAXS patterns.

A quantitative analysis of the domains (based on a Voronoi tessellation) was then performed using TRAVIS software.[63,64] In the mixtures of ACN, acetone, THF and DMF with 5.0 M water and 0.1 M $LiClO_4$, the average calculated size of the aqueous (H_2O + $LiClO_4$) domains is 315.2, 376.9, 339.3 and 55.9 Å^3, respectively (Figure 4a). As can be seen on the snapshots, the shape of the aqueous domains in the mixtures with ACN, acetone and THF is not spherical (average isoperimetric quotient of ~ 0.65 whereas spherical domains would give a quotient value close to 1).

Furthermore, isolated water molecules coexist with large domains (> 30 water molecules) at a given time. Considering the molecular volume of liquid water at ambient temperature (29.9 $Å^3$) and omitting $LiClO_4$ (there are 50 times more water molecules than $LiClO_4$ in the boxes), these volumes correspond to an average of 10.5, 12.6, 11.3 and 1.9 water molecules per domain, respectively. Consequently, the number of water-water hydrogen bonds is much smaller in the DMF-based mixture compared to the other mixtures in which aqueous nanodomains are present (Figure 4b). Although not directly comparable due to different numbers of solvent molecules per system (Tables S1-4), the DMF-H_2O hydrogen bonds are more numerous than the other solvent-water hydrogen bonds (Figure S29). In the mixtures in which aqueous nanodomains are present, water molecules are surrounded by ~ 2.0 – 2.4 water molecules in their first solvation shell (Figure 4c and S30). On the contrary, in the mixture with DMF, the first solvation shell of water molecules only contains ~ 0.8 water molecules. Water molecules are replaced with DMF molecules due to the formation of strong hydrogen bonds between water and the oxygen atom of DMF (Figure S29 and S31). Water molecules are therefore found in average as isolated molecules or dimers in the DMF mixture. As mentioned earlier, a few simulation[57,58] and experimental studies[59,60] report some degree of heterogeneity in DMF/water mixtures, especially around equimolar ratios. As discussed in the Supplementary Discussion 1, the degree of heterogeneity found in MD simulations greatly depends on the force fields; to avoid such pitfall we selected our force fields to reproduce as best as possible the experimental SAXS patterns, i.e., the structure in the mixtures. Moreover, the existence of relatively large water and DMF aggregates were proposed based on IR Spectroscopy measurements.[59] At a DMF molar fraction of 0.7 (as in DMF/5.0 M H_2O/0.1 M $LiClO_4$) the authors found that the fraction of water -OH bonds hydrogen-bonded to other water molecules and to DMF molecules is equal to ~ 20% and ~ 80%, respectively. From our simulation

which shows that water molecules are homogeneously distributed in the mixture with DMF, we find the exact same fraction of water molecules hydrogen-bonded to DMF and water molecules (Figure S32). That being said, our results only hold for DMF/5.0 M water mixtures and the existence of large aqueous domains cannot be excluded at other water molar fractions.

Overall, our combined experimental and MD simulation results demonstrate the existence of relatively large aqueous nanodomains containing a dozen of water molecules in average in the mixtures of ACN, acetone and THF with 5.0 M water and 0.1 M $LiClO_4$. On the contrary, due to the presence of strong water-DMF hydrogen bonds, water molecules are homogeneously distributed in the mixture with DMF and exist in average as isolated molecules or dimers.

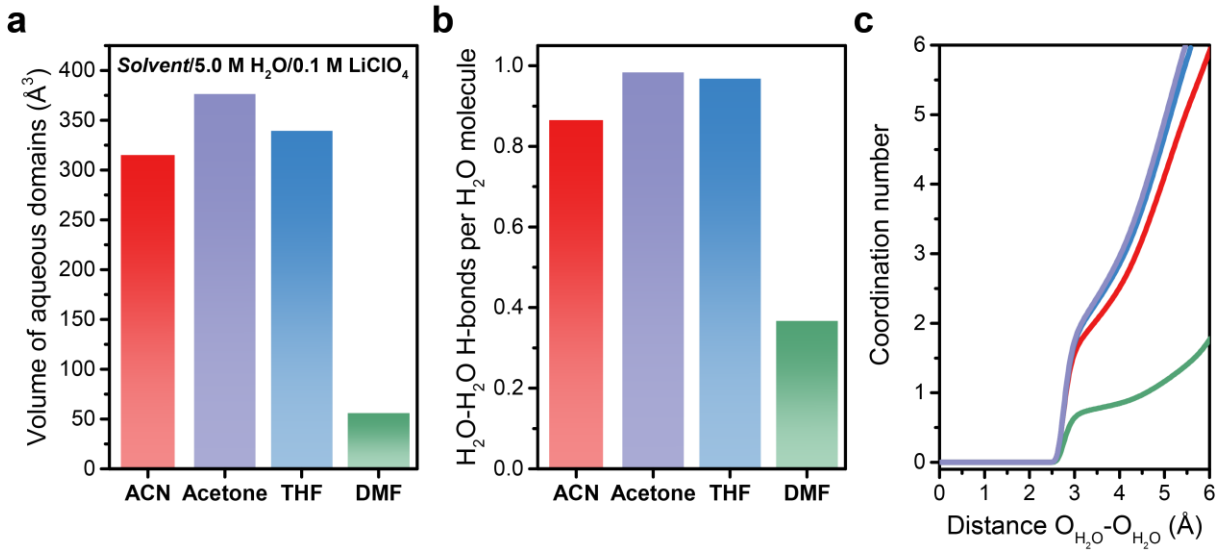

Figure 4. (a) Average volume of aqueous (H_2O + $LiClO_4$) domains and (b) average number of water-water hydrogen bonds per water molecule in solvent/5.0 M water/0.1 M $LiClO_4$ mixtures. (c) Coordination numbers for O_{H2O}-O_{H2O} as obtained from the corresponding O_{H2O}-O_{H2O} radial distribution functions. The hydrogen bonds were computed using the following geometrical criteria: $d(D-A) \leq 3.5$ Å and $\alpha(HDA) \leq 30°$ with $d(D-A)$ the distance between the hydrogen bond donor (D) and acceptor (A) atoms and $\alpha(HDA)$ the angle defined by the hydrogen atom (H) bonded to D, D and A with D being the vertex. All the possible hydrogen bond donor and acceptor atoms of water molecules are considered in the calculation.

Water reactivity at electrified interfaces.

Having demonstrated that organic solvents can be used to tune aqueous heterogeneities in hybrid organic solvent/water electrolytes, our attention then turned to the effect of the resulting modification of the structure of water on its electrochemical reactivity. A common pitfall when describing the reactivity of water in complex solutions, which include superconcentrated aqueous electrolytes or binary mixtures with organic solvents, is the difficulty in estimating the reversible hydrogen potential to accurately evaluate the kinetics of the HER and the OER due to the lack of robust and reliable potential reference. The ferrocenium/ferrocene couple ($Fc^{+/0}$) is commonly used as an internal reference in organic electrochemistry. However, while the use of $Fc^{+/0}$ is adequate for potentials measured in a single solvent, several studies have pointed out that its redox potential is dependent on the supporting salt and the solvent.[65–68] This dependence primarily arises from ion-pairing forming between ferrocenium (Fc^{+}) and supporting salt anions, which occurs to a large extent in low permittivity solvents, as probed spectroscopically.[68] Permethylated derivatives of ferrocene, in particular decamethylferrocene ($Me_{10}Fc$), have been proposed as better internal references for comparing potentials in different solvents.[65–67] Indeed, their bulkier structure can isolate more efficiently the iron redox center from interactions with the solvent molecules and supporting salt ions.[65–67] We thus first estimated the redox potential of $Me_{10}Fc^{+/0}$ in solvent/5.0 M water mixtures and compared it to the redox potential of $Fc^{+/0}$ in the same mixtures. The difference between the $Me_{10}Fc^{+/0}$ and $Fc^{+/0}$ redox potentials [$\Delta E_{1/2}$ ($Fc^{+/0}$ – $Me_{10}Fc^{+/0}$)] only slightly depends on the concentration of supporting salt but strongly depends on the organic solvent (Figure 5), in very good agreement with values found for the pure solvents.[66] This suggests that the redox potential of at least one of the redox couples is dependent on the supporting salt/solvent. Strikingly, $\Delta E_{1/2}$ ($Fc^{+/0}$ – $Me_{10}Fc^{+/0}$) is in the same order of magnitude for the mixtures with high permittivity

solvents (ACN: 37.5, acetone: 20.7 and DMF: 36.7) whereas it is much lower for the mixture with THF, which has a lower permittivity (7.5). The dependence of $\Delta E_{1/2}$ ($Fc^{+/0}$ – $Me_{10}Fc^{+/0}$) on the supporting salt/solvent therefore likely arises from a shift of the $Fc^{+/0}$ redox potential due to Fc^{+}-anion pairing; nevertheless, a shift of the $Me_{10}Fc^{+/0}$ redox potential cannot be completely excluded. In the following, we reference our electrochemical data against both redox couples for comparison.

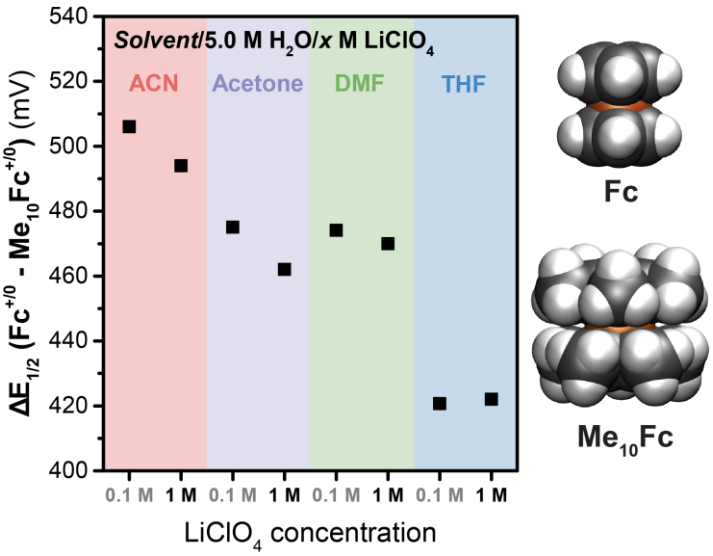

Figure 5. $E_{1/2}$ difference between the $Fc^{+/0}$ and the $Me_{10}Fc^{+/0}$ couples for different mixtures studied in the present work. $E_{1/2}$ corresponds to the halfway potential between the anodic and cathodic peaks observed on the cyclic voltammograms of the corresponding redox couples. $E_{1/2}$ is a very good approximation of the formal potentials of the couples. The $\Delta E_{1/2}$ values were obtained by performing cyclic voltammetry at glassy carbon electrodes (100 $mV.s^{-1}$) of 0.5 mM Fc + 0.5 mM $Me_{10}Fc$ in the different mixtures. See Table S5 for $\Delta E_{1/2}$ values for a larger number of mixtures. The values are in very good agreement with the values obtained for the pure solvents.[66] Right: Van Der Waals sphere structures of Fc and $Me_{10}Fc$.

To probe the electrochemical reactivity of water, HER measurements at polycrystalline platinum electrodes and OER ones at polycrystalline gold electrodes were carried out in solvent/5.0 M water/0.1 M $LiClO_4$ electrolytes (Figure 6). Note that HER data could not be obtained in THF/water mixtures as a parasitic reaction occurs before the HER at Pt electrodes (Figure S33). Similarly, OER data could not be reliably obtained in DMF and THF/water mixtures as both

solvents oxidize at potentials close to the OER (Figure S34). For both the HER and OER, referencing potentials against $Me_{10}Fc^{+/0}$ instead of $Fc^{+/0}$ does not lead to significant changes. The HER in the mixture with DMF occurs at potentials ~ 250 mV vs $Fc^{+/0}$ more negative than that in the mixture with acetone and ~ 350 mV vs $Fc^{+/0}$ more negative than with ACN (the shifts are slightly higher when referenced against $Me_{10}Fc^{+/0}$ – Figure 6a,b and Figure S35). Strikingly, the reactivity trend for the OER in the acetone and ACN-based mixtures is the exact opposite of the trend observed for the HER, with the OER in the mixture with ACN occurring at potentials ~ 100 mV vs $Fc^{+/0}$ more positive than with acetone (Figure 6c,d).

As studied in depth in the field of OER and HER, strong Lewis cations such as Li^+ greatly impact the reactivity of water at electrochemical interfaces. Li^+ cations were found to be detrimental to the OER due to the strong Li^+-OH_2 interaction and conversely activate the HER (weakening of the O-H bond).[6,7,32] Therefore, the reactivity trend observed in the acetone and ACN-based mixtures could be tentatively explained by a greater amount of Li^+-OH_2 interactions in the ACN mixtures when compared with the acetone one. However, this hypothesis can be discarded as the trend obtained in mixtures containing hydrophobic tetrabutylammonium (TBA^+) cations in place of Li^+ is identical (Figure S36), with both reactions shifted in an exact opposite way in acetone and ACN-based mixtures. More strikingly, gold dissolution into the electrolyte, an event expected to be independent of the structure of water and which occurs before the OER in organic solvent/water mixtures,[16] is also shifted in the same order of magnitude as function of the electrolyte composition (Figure S37). Taken as a whole, these observations point toward a shift in thermodynamic potential rather than a change in kinetics to explain the observed trend for the OER and the HER in acetone and ACN-based mixtures.

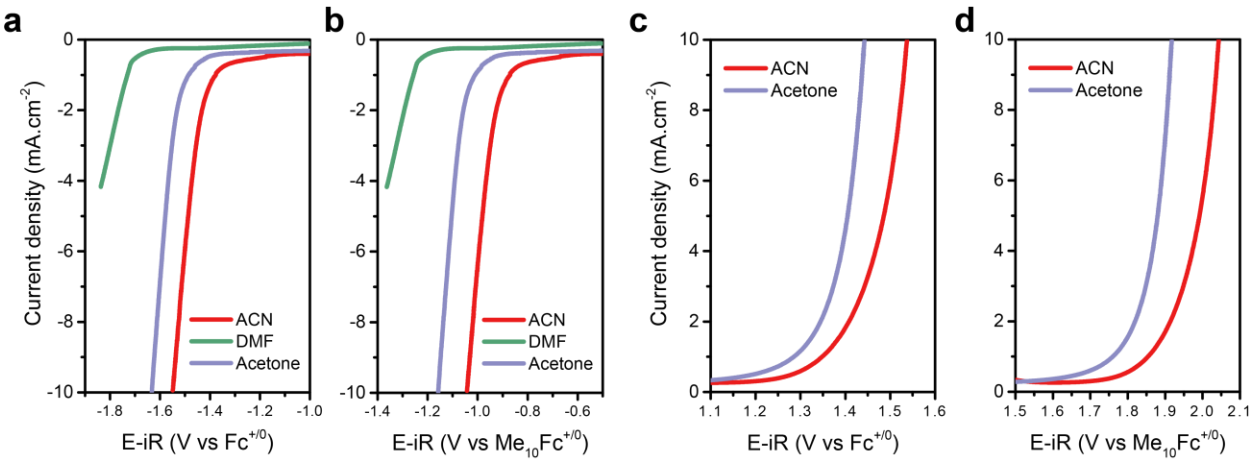

Figure 6. HER performed at polycrystalline platinum rotating disk electrodes (RDE) (a,b) and OER performed at polycrystalline gold RDE (c,d) in ACN (red), DMF (green) and acetone (purple) mixtures with 5.0 M H_2O and 0.1 M $LiClO_4$. The electrochemical curves are referenced versus the $Fc^{+/0}$ couple (a,c) or the $Me_{10}Fc^{+/0}$ couple (b,d). Working electrode (WE): polycrystalline Pt or Au RDE, Counter electrode (CE): Pt wire, Ref: leakless Ag/AgCl, Ar-saturated solvent/5.0 M water/0.1 M $LiClO_4$, 25°C, 50 $mV.s^{-1}$, 1,600 rpm.

To conclude on the origin of the shifts observed in the different mixtures, we first examined the hydrogen oxidation reaction (HOR). When referencing against $Fc^{+/0}$ and $Me_{10}Fc^{+/0}$, the HOR and HER curves in the mixtures with acetone and ACN are, once again, shifted in an exact opposite way (Figure 7a,b). To verify if the observed shifts arise from a shift of the H_2O/H_2 thermodynamic potential, we experimentally measured the equilibrium potential of a platinum rotating disk electrode rotated at 2,500 rpm[69] immerged in H_2-saturated solvent/5.0 M water/0.1 M $LiClO_4$ mixtures, constituting a reversible hydrogen electrode (RHE) (see Experimental section and Figures S38-40 for full details). When referenced against RHE, no shift is observed for the HER and HOR curves between the acetone and ACN-based mixtures (Figure 7c). This unambiguously confirms that the previously observed shift when referencing against $Fc^{+/0}$ and $Me_{10}Fc^{+/0}$ arises from a shift of the H_2O/H_2 thermodynamic potential. Accordingly, when referenced against RHE, no shift is observed for the OER curves in both mixtures (Figure S41). These results are in

accordance with our SAXS and MD results which showed that the nanostructure in ACN and acetone/5.0 M water mixtures is similar, both exhibiting the presence of relatively large aqueous domains. However, in the mixture with DMF, in which water and DMF mix with each other on the molecular scale, the HER occurs at ~ 100 mV vs RHE more negative potentials than in the two mixtures that contain large aqueous domains (Figure 7c). This trend is preserved at constant molar fraction of water (Figure S42). To confirm this effect, an electrolyte composed of dimethylsulfoxide (DMSO) and water, which mix at the molecular scale due to the establishment of hydrogen bonds that are stronger than the DMF-water ones[31,43,44,70–72] (Figure S1 and S6a), was tested. Accordingly, the HER occurs at even more negative potentials in the DMSO/5.0 M water mixture (Figure S43). Therefore, we conclude based on these results that the reduction of water is more facile in the presence of large aqueous domains. This observation can be rationalized by previous reports suggesting that several layers of water are required to accomplish the Volmer step ($H_2O + e^- = H_{ads} + HO^-$) and evacuate OH^- ions from the electrode surface following a Grotthuss diffusion mechanism.[32,73–76] In addition to the establishment of aqueous heterogeneities, short-range cation-water interactions can also impact the reactivity of water at electrified interfaces, as previously observed for ACN/water mixtures,[32] and confirmed following this methodology. Indeed, when referenced against the experimentally determined RHE, the increase of $LiClO_4$ concentration is found to induce a decrease of the HER onset potential (due to the weakening of O-H bonds by the strong Li^+-OH_2 interaction) while being detrimental to the OER. Instead, the use of large and hydrophobic cations such as TBA^+ prevents water from accessing the surface under cathodic polarization and thus slows down the HER (Figures S44-47). Our results demonstrate that the clustering of water molecules, which is controlled by the strength of the hydrogen bonding with organic solvent molecules, drastically impacts the electrochemical

reactivity of water. More importantly, we show that careful referencing against RHE is pivotal to accurately probe and compare the reactivity of water in different mixtures.

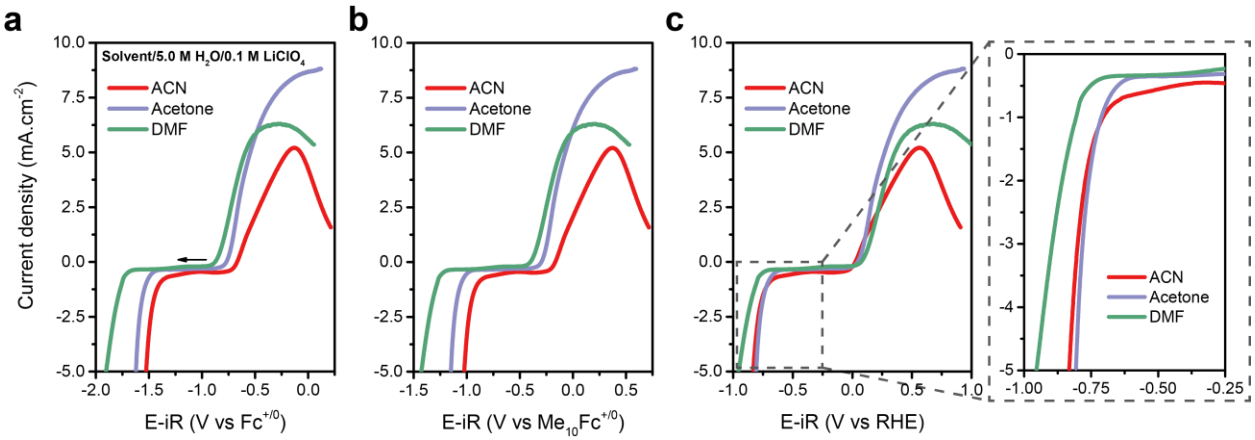

Figure 7. HOR and HER measurements at polycrystalline platinum electrodes in ACN (red), DMF (green) and acetone (purple) mixtures with 5.0 M H_2O and 0.1 M $LiClO_4$. The electrochemical curves are referenced against (a) the $Fc^{+/0}$ couple, (b) the $Me_{10}Fc^{+/0}$ couple and (c) RHE. The arrow in panel a indicates the sweep direction. The variations in HOR current densities are due to the different mass transport properties of the mixtures and different $H_{2(g)}$ solubility in the mixtures. WE: polycrystalline Pt RDE, CE: Pt wire, Ref: leakless Ag/AgCl, H_2-saturated solvent/5.0 M water/0.1 M $LiClO_4$, 25°C, 50 $mV.s^{-1}$, 1,600 rpm.

Effect on electrosynthetic reactions.

Having demonstrated that the electrochemical reactivity of water is modulated in hybrid electrolytes by its solvation structure at short to intermediate range, we then investigated if similar effect of the water structure can control the outcome of electrosynthetic reactions. Indeed, the hybrid electrolytes herein studied are state of the art electrolytes used for reactions in which water acts either as the oxygen-atom source in anodic reactions[16–24] or as the proton/deuterium source in cathodic reactions.[23,25–27] Here, we examine two recently developed electrosynthetic reactions, the electrochemical oxidation of sulfides[20,24] and the deuteration of benzylic halides.[27] Thioanisole oxidation and benzyl bromide reduction at glassy carbon (GC) electrodes are selected as model reactions (Scheme 1). Both reactions proceed first by the oxidation/reduction of the organic

substrate, which generates an intermediate that subsequently chemically reacts with water. The electrochemical oxidation of thioanisole generates a radical cation centered on the sulfur atom following a one-electron process.[20,24] The sulfoxide product is obtained after chemical reaction with water and subsequent oxidation and deprotonation. Instead, the electrochemical reduction of benzyl bromide proceeds *via* a two-electron process giving the corresponding carbanion (Scheme 1).[77] The reduction is a two-electron process because the reduction potential of the neutral radical formed after the dehalogenative one-electron reduction of benzyl bromide is more positive than the reduction potential of benzyl bromide itself.[77,78] The carbanion subsequently reacts with D_2O to form (methyl-d_1)benzene.

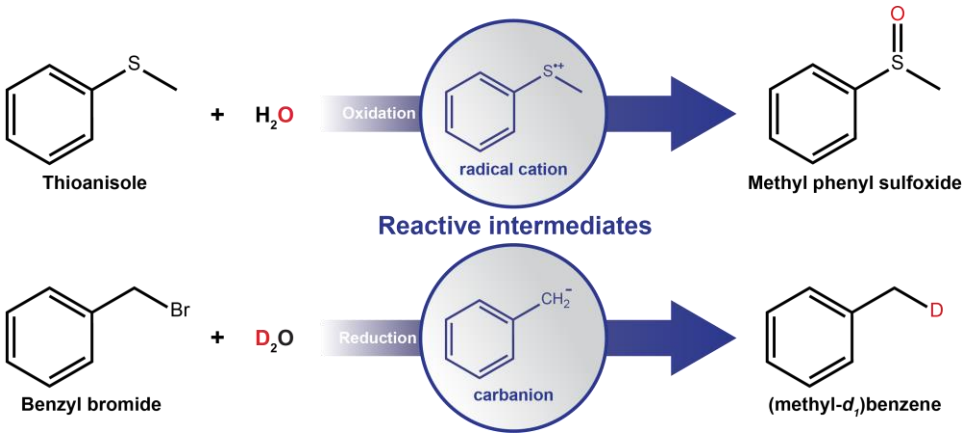

Scheme 1. Top: Electrochemical oxidation of thioanisole into its sulfoxide with water as the oxygen source. Down: Electrochemical deuteration of benzyl bromide with heavy water as the deuterium source.

The cyclic voltammograms of the oxidation of thioanisole and the reduction of benzyl bromide at GC electrodes show that no significant shifts of onset potential are observed between the different mixtures (Figure 8). Only variations in current intensities are observed, which are due to the different mass transport properties of the mixtures (Figure S48). This result can be rationalized by observing that the intermediates formed for both reactions are highly reactive, as probed by fast-scan voltammetry (Figure S49). Indeed, for such reactions where the initial electron transfer is

totally irreversible, the following chemical reaction causes no change in characteristic potential.[79] Hence, in such case, the nanoscale structure of water will not impact the kinetics of the overall electrochemical reaction. One can note that the choice of internal reference, i.e., $Fc^{+/0}$ or $Me_{10}Fc^{+/0}$ (referencing against RHE is meaningless here as water is not the reactant at the electrode), leads to small ~ 10 – 20 mV variations in onset potential (Figure 8). Therefore, from one solvent system to another, small shifts of onset potential in the order of 10 – 20 mV can hardly be attributed to differences in reactivity and discussing such small shifts should be avoided.

Our results allow us to classify reactions occurring in hybrid organic solvent/water electrolytes in two categories, as function of the mechanism, i.e., if water is the reactant at the electrode or if it chemically reacts with highly reactive electrogenerated intermediates. When water reacts first at the electrode, the kinetics of the reaction is sensitive to the existence and the composition of aqueous heterogeneities in the organic solvent, as demonstrated for the HER and the OER. Hence, for electrosynthetic reactions in which water reacts first at the electrode, such as for the deuteration of alkynes at Pd electrodes,[26] a modulation of the onset potential by the structure of water is expected, which can only be quantitatively understood by referencing against the RHE. When a highly reactive electrogenerated intermediate is first generated before to react with water, the overall kinetics of the reaction is not affected by the structure of water in hybrid electrolytes as observed for benzyl bromide reduction or thioanisole oxidation (Figure 8). Indeed, for such reactions where the initial electron transfer is totally irreversible, the following chemical reaction does not modulate the onset potential. However, one cannot exclude a modulation of product selectivity in such case, due to interactions with intermediates/products and different mass transport effects or double layer effects.

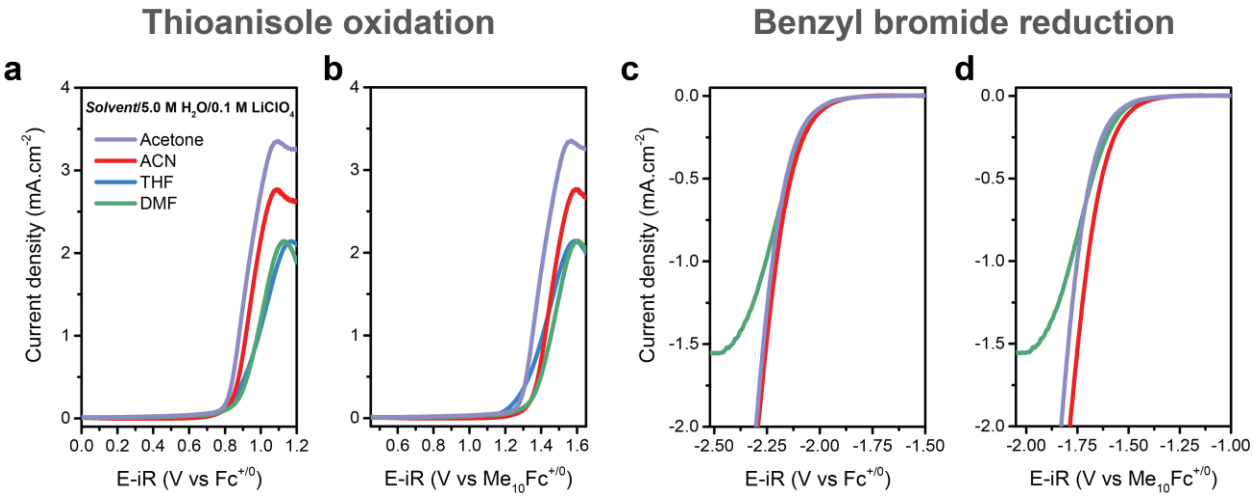

Figure 8. Cyclic voltammograms obtained at a rotating GC electrode in organic solvent/5.0 M water/0.1 M $LiClO_4$ mixtures in the presence of 1.0 mM thioanisole (a,b) and 1.0 mM benzyl bromide (c,d). Cyclic voltammograms are background-subtracted and are referenced versus the $Fc^{+/0}$ couple (a,c) or the $Me_{10}Fc^{+/0}$ couple (b,d). The variations in current intensities are due to the different mass transport properties of the mixtures. The peak observed for the oxidation of thioanisole is likely due to product adsorption at the GC electrode. WE: GC, CE: Pt wire, Ref: leakless Ag/AgCl, Ar-saturated solvent/5.0 M water/0.1 M $LiClO_4$ with 1.0 mM thioanisole or 1.0 mM benzyl bromide, 25°C, 50 $mV.s^{-1}$, 1,600 rpm.

CONCLUSIONS

In summary, through a comprehensive characterization of four synthetically-relevant mixtures and careful electrochemical measurements, we have rationalized the effect of the electrolyte structure on the outcome of electrochemical reactions performed in hybrid electrolytes. To get insights into the structure of water in the electrolytes, synchrotron SAXS measurements were performed in combination with MD simulations. A comprehensive investigation of force fields for the solvents allowed us to accurately reproduce the experimental SAXS patterns both at short and intermediate range. Our combined experimental and simulation results show the existence of relatively large aqueous nanodomains containing a dozen of water molecules in average in the mixtures of ACN, acetone and THF with 5.0 M water. On the contrary, due to the formation of strong water-DMF hydrogen bonds, water molecules were found to be homogeneously distributed in the mixture with

DMF and to exist, in average, as isolated molecules or dimers. We have demonstrated that water in aqueous domains is more reactive for the HER than isolated water molecules, in agreement with previous reports suggesting that several layers of water are required to accomplish the Volmer step and evacuate OH^- ions from the electrode surface following a Grotthuss diffusion mechanism.[32,73–76] Importantly, our careful analysis of potential referencing unambiguously revealed that the variation in the reactivity of water upon formation of aqueous nanodomains originates from a kinetic effect rather than a thermodynamic shift due to a change in water activity. Our methodology allowed us to confirm that short-range cation-water interactions can also impact the reactivity of water at electrified interfaces, as previously observed for ACN/water mixtures.[32] Comparing the results obtained for the reactivity of water with those collected from two recently developed electrosynthetic reactions (the electrochemical oxidation of sulfides and the electrochemical deuteration of benzylic halides),[20,24,27] we classify electrochemical reactions performed in hybrid electrolytes in two categories. For reactions proceeding *via* the activation of water first, such as for the HER, OER or the deuteration of alkynes at Pd electrodes, fine tuning of aqueous domains in hybrid electrolytes will impact the kinetics of the reaction. Instead, when organic substrates react at the electrode prior to water, *e.g.* for the oxidation of sulfides or the reduction of organic halides, aqueous domains will have no impact on reaction kinetics. The knowledge gathered in the present study can be used to modulate numerous electrosynthetic reactions. For instance, our results show that performing reactions in DMF/5.0 M water mixtures allows for slowing down the HER while leaving unaffected reduction/oxidation potentials of organic substrates, which could help minimizing the competing HER in the electrohydrodimerization of acrylonitrile for instance.[12,13] We believe that such detailed investigation of the solvation properties of hybrid electrolytes can be transposed to other electrosynthetic reactions and help tune kinetics and product

selectivities. Nevertheless, further development of the field will only be achieved by gaining further insights regarding reaction intermediates forming in such hybrid electrolytes at the catalyst interface and investigations on interfacial solvation structures are thus needed.

EXPERIMENTAL SECTION

Reagents. Acetone (RE-pure) was purchased from Carlo Erba. Acetonitrile (99.9%, Extra Dry over Molecular Sieves, AcroSeal) was purchased from Acros Organics. Benzyl bromide (99%), lithium perchlorate (anhydrous, 99%), tetra-n-butylammonium perchlorate (electrochemical grade) and tetramethylsilane (99.9%) were purchased from Alfa Aesar. Decamethylferrocene (99%) was purchased from Strem Chemicals. DMSO (99+%) and DMF (99.8%, extra dry, AcroSeal) were purchased from Thermo Fisher Scientific. Ferrocene (99%), tetrahydrofuran (anhydrous, >99.9%, inhibitor-free) and thioanisole (ReagentPlus, >99%) were purchased from Sigma-Aldrich. Milli-Q water (18.2 MΩ.cm at 25°C) was used for electrolytes containing water.

Electrochemical measurements (general). Data were acquired on a BioLogic VSP potentiostat. All electrochemical measurements were recorded using a three-electrode cell setup with a leakless Ag/AgCl (ET069, diam. 5 mm, L 100 mm, eDAQ, provided by Mengel Engineering) reference electrode. A flame-annealed platinum wire was used as a counter electrode and placed in a separate compartment. All electrochemical measurements were conducted in a jacketed electrochemical cell to perform the experiments at constant temperature (25°C). Prior to any measurement, glassy carbon, polycrystalline gold and polycrystalline platinum electrodes (5 mm diameter, 0.196 cm^2 geometric surface area, Pine research) were polished with three polishing slurries (6 µm diamond on nylon polishing disc, followed by 0.3 µm and 0.04 µm aluminum oxide on micro-cloth polishing disc) using a polishing machine (Le Cube, Presi). Residual traces of slurries were

removed by sonicating the as-polished electrodes three times in water (1 min each) and one time in acetone (1 min). Polycrystalline platinum electrodes were further electrochemically cleaned by the following procedure: 2 min potential hold at + 2.0 V vs RHE (under rotation at 1,600 rpm) in an Ar-saturated 0.5 M H_2SO_4 solution followed by 20 cycles of CV between -0.15 and 1.60 V vs RHE at 500 $mV.s^{-1}$. Then, 10 cycles of CV between 0.0 and 1.35 V vs RHE at 100 $mV.s^{-1}$ were performed to check the cleanliness of the electrode (Figure S50). The freshly cleaned electrodes were rinsed with ultrapure water and air-dried. The ohmic drop was measured by electrochemical impedance spectroscopy (EIS) after electrochemical measurements. Typical values of around 25 to 250 Ω were obtained, depending on the supporting salt concentration and the solvent. The ohmic drop compensation was performed manually during the data treatment (85% of correction). To remove metallic impurities, the cell and the separate compartment for the counter electrode were regularly washed with aqua regia and to remove organic impurities they were regularly washed with $KMnO_4/H_2SO_4$ (1 $g.L^{-1}$ $KMnO_4$ dissolved in 0.5 M H_2SO_4) solution followed by a diluted 1:1 H_2O_2/H_2SO_4 solution.

RHE reference. A platinized platinum wire was first used to accurately measure the equilibrium potential.[69] However, the measured potential was found to be unstable (Figure S38) and a fade of the black color of the wire was noticeable after the measurements. A platinum RDE rotated at 2,500 rpm was therefore used,[69] giving stable potentials (Figure S39). Great care was taken when cleaning the RDE before measurements as the measured potentials are sensitive to the cleanliness of the electrode (Figure S40).

Fast scan cyclic voltammetry. Fast scan CVs were obtained using homemade 0.5 mm diameter Pt electrode for thioanisole oxidation and 0.5 mm diameter carbon fiber electrode for benzyl bromide reduction (Figure S49). The electrodes were made by inserting a 0.5 mm diameter Pt or

carbon fiber wire into a 0.5 mm inner diameter PEEK tube (Interchim) filled with epoxy resin. The electrodes were let to dry overnight and the tip was cut to make sure no residue of epoxy resin was left on the electrode surface. EC-Lab Express software was used to allow for a higher sampling rate and data were acquired on a BioLogic VSP potentiostat.

Preparation of electrolyte solutions. All electrolyte solutions were prepared in 10 mL volumetric flasks before measurements. 106.4 mg and 1064.0 mg of $LiClO_4$ were added into the volumetric flask to prepare the different mixtures containing 0.1 M and 1.0 M $LiClO_4$. 341.9 mg of $TBAClO_4$ were added into the volumetric flask to prepare the different mixtures containing 0.1 M $TBAClO_4$. 900 µL of Milli-Q water were added into the flask for mixtures containing 5.0 M water. The flasks were completed up to ~ 2 mm below the ring graduation with the corresponding organic solvent and let to rest for ~ 10 min to allow for temperature equilibration (the mixtures of the different solvents with water are either exothermic or endothermic). The flasks were subsequently completed to the ring graduation. Mixtures with fixed water molar fraction were prepared by mixing given volumes of organic solvent and water (determined from the molar volumes of the solvents and water) in a separate flask. The as-obtained mixture was subsequently added into a flask containing the supporting salt. Depending on the experiment, the organic solvents and water were separately saturated with Ar or H_2 before the preparation of the mixtures.

Infrared spectroscopy. IR spectra were acquired on a Shimadzu IRPrestige-21 spectrometer.

Nuclear magnetic resonance spectroscopy. Liquid-state NMR spectra were recorded on a Bruker 7.046 T Avance III HD NMR spectrometer mounted with a 5 mm HX(F) probehead. NMR tubes were equipped with a coaxial insert filled with D_2O (99% D, Sigma-Aldrich) to lock the magnetic field. Tetramethylsilane was used as an internal reference.

Small-angle X-ray scattering (SAXS). SAXS patterns were collected at the SWING beamline (SOLEIL synchrotron, Saint-Aubin, France). The beamline was operated at 16 keV and an Eiger 4 M Detector (Dectris) was used. SAXS patterns of empty 1.5 mm capillaries were first measured and then the electrolyte samples were filled into the corresponding capillaries, sealed with Parafilm and subsequently measured. The measurements were performed at room temperature (5 s acquisition time). The sample-to-detector distances were set to 6.2 m and 0.5 m, covering the scattering vectors in the range from q = 0.0013 to 2.53 $Å^{-1}$. Background subtraction was performed manually after the measurements. The commercial acetonitrile bottles used in the present study contain molecular sieves for dryness. Therefore, the acetonitrile was centrifuged at 6,000 rpm for 10 min before preparation of the solutions to avoid any effect of potential molecular sieve dust on the SAXS signal.

Molecular dynamics simulations. Force field-based MD simulations of the bulk electrolytes were performed using the GROMACS software package.[80] All the force fields were carefully chosen to reproduce as best as possible the experimental SAXS patterns, i.e. the bulk structure of the mixtures (see Supplementary Information 1 for full details). Mixed Lennard–Jones parameters for all of the different atom types were obtained using the Lorentz–Berthelot combination rules. The simulations were performed in the NVT ensemble at 300 K for 75 ns using the Nosé-Hoover thermostat[81,82] (relaxation time of 0.5 ps) with a timestep of 1 fs and saving configurations every 1 ps. The number of each species in the boxes and the size of the boxes were calculated to match the experimental densities (the physical properties of the different electrolytes and the corresponding box configurations are given in Tables S1-4). The initial configuration was obtained by generating a cubic box using the PACKMOL package[83]. The systems were equilibrated in the NVT ensemble at 700 K for 5 ns prior to the simulations at 300 K. Large ~ 100 * 100 * 100 $Å^3$

boxes were used in order to simulate SAXS patterns at low q (up to 0.0628 $Å^{-1}$ in that case) while maintaining reasonable computational times. Long-range electrostatic interactions were computed with the particle mesh Ewald method, while a cut-off of 12 Å was adopted for the non-bonded interactions. The LINCS algorithm was employed to constrain the stretching interactions involving hydrogen atoms. The analyses were performed on the last 50 ns with GROMACS utilities. The analysis of aqueous domains was performed on the last 10 ns with TRAVIS[63,64,84] and the SAXS patterns were simulated on the last 2 ns with GROMACS utilities.[85] The size of the aqueous domains computed with TRAVIS is not dependent on the size of the box (as long as it is not too small). Indeed, their volume in the ACN/water mixture is identical to those found in our previous studies on ACN/water mixtures in which we used 12 times smaller boxes (~ 44 Å cell length compared to 100 Å here).[16,32] VMD software was used to visualize boxes and generate snapshots.[86]

ASSOCIATED CONTENT

Additional experimental (synchrotron SAXS, IR, NMR, electrochemical data) and MD simulations data to support the results of the main text (Figures S1-S50, Tables S1-S5).

AUTHOR INFORMATION

Corresponding Author

Alexis Grimaud – Department of Chemistry, Merkert Chemistry Center, Boston College, Chestnut Hill, MA; Chimie du Solide et de l'Energie, UMR 8260, Collège de France, 75231 Paris Cedex 05, France ; Réseau sur le stockage Electrochimique de l'Energie (RS2E), CNRS FR3459, 80039 Amiens Cedex, France ; https://orcid.org/0000-0002-9966-205X; Email: alexis.grimaud@bc.edu

Authors

Florian Dorchies – Chimie du Solide et de l'Energie, UMR 8260, Collège de France, 75231 Paris Cedex 05, France; Sorbonne Université, France; Réseau sur le stockage Electrochimique de

l'Energie (RS2E), CNRS FR3459, 80039 Amiens Cedex, France ; https://orcid.org/0000-0003-2300-7582

Alessandra Serva – Réseau sur le stockage Electrochimique de l'Energie (RS2E), CNRS FR3459, 80039 Amiens Cedex, France; Sorbonne Université, CNRS, Physicochimie des Électrolytes et Nanosystèmes Interfaciaux, PHENIX, F-75005 Paris, France; https://orcid.org/0000-0002-7525-2494

Astrid Sidos – Department of Chemistry, Merkert Chemistry Center, Boston College, Chestnut Hill, MA; Chemistry Department, École Normale Supérieure, PSL University, 75005 Paris, France

Laurent Michot – Sorbonne Université, CNRS, Physicochimie des Électrolytes et Nanosystèmes Interfaciaux, PHENIX, F-75005 Paris, France; https://orcid.org/0000-0002-0519-6992

Michaël Deschamps – Réseau sur le stockage Electrochimique de l'Energie (RS2E), CNRS FR3459, 80039 Amiens Cedex, France; CNRS, CEMHTI, UPR 3079, Université d'Orléans, F-45071 Orléans, France; https://orcid.org/0000-0001-8309-3932

Mathieu Salanne – Réseau sur le stockage Electrochimique de l'Energie (RS2E), CNRS FR3459, 80039 Amiens Cedex, France; Sorbonne Université, CNRS, Physicochimie des Électrolytes et Nanosystèmes Interfaciaux, PHENIX, F-75005 Paris, France; Institut Universitaire de France (IUF), 75231 Paris, France; https://orcid.org/0000-0002-1753-491X

AUTHORS CONTRIBUTION

The manuscript was written through contributions of all authors. All authors have given approval to the final version of the manuscript.

ACKNOWLEDGEMENTS

F.D. thanks the École normale supérieure Paris-Saclay for his PhD scholarship. The Ecole Normale Supérieure (Paris, https://www.chimie.ens.fr/?q=en) is gratefully acknowledged for financial support for A.Sidos internship. The authors acknowledge HPC resources granted by the SACADO service unit of Sorbonne University, France. The authors acknowledge SOLEIL for provision of synchrotron radiation facilities and would like to thank Thomas Bizien for assistance

in using the SWING beamline. The authors thank Cédric Leau for useful discussions on ATR IR spectroscopy.

Notes

The authors declare no competing interests.

The input files used for the molecular dynamics simulations are openly available in the repository to be added after acceptance.

REFERENCES

(1) Dorchies, F.; Grimaud, A. Fine Tuning of Electrosynthesis Pathways by Modulation of the Electrolyte Solvation Structure. *Chem. Sci.* **2023**, *14* (26), 7103–7113. https://doi.org/10.1039/d3sc01889j.

(2) Schreier, M.; Kenis, P.; Che, F.; Hall, A. S. Trends in Electrocatalysis: The Microenvironment Moves to Center Stage. *ACS Energy Lett.* **2023**, *8* (9), 3935–3940. https://doi.org/10.1021/acsenergylett.3c01623.

(3) Lucky, C.; Schreier, M. Mind the Interface: The Role of Adsorption in Electrocatalysis. *ACS Nano* **2024**, *18* (8), 6008–6015. https://doi.org/10.1021/acsnano.3c09523.

(4) Bender, J. T.; Petersen, A. S.; Østergaard, F. C.; Wood, M. A.; Heffernan, S. M. J.; Milliron, D. J.; Rossmeisl, J.; Resasco, J. Understanding Cation Effects on the Hydrogen Evolution Reaction. *ACS Energy Lett.* **2023**, *8* (1), 657–665. https://doi.org/10.1021/acsenergylett.2c02500.

(5) Monteiro, M. C. O.; Goyal, A.; Moerland, P.; Koper, M. T. M. Understanding Cation Trends for Hydrogen Evolution on Platinum and Gold Electrodes in Alkaline Media. *ACS Catal.* **2021**, *11* (23), 14328–14335. https://doi.org/10.1021/acscatal.1c04268.

(6) Yang, C.; Fontaine, O.; Tarascon, J. M.; Grimaud, A. Chemical Recognition of Active Oxygen Species on the Surface of Oxygen Evolution Reaction Electrocatalysts. *Angew. Chemie - Int. Ed.* **2017**, *56* (30), 8652–8656. https://doi.org/10.1002/anie.201701984.

(7) Görlin, M.; Halldin Stenlid, J.; Koroidov, S.; Wang, H.-Y.; Börner, M.; Shipilin, M.; Kalinko, A.; Murzin, V.; Safonova, O. V.; Nachtegaal, M.; Uheida, A.; Dutta, J.; Bauer, M.; Nilsson, A.; Diaz-Morales, O. Key Activity Descriptors of Nickel-Iron Oxygen Evolution Electrocatalysts in the Presence of Alkali Metal Cations. *Nat. Commun.* **2020**, *11* (1), 6181. https://doi.org/10.1038/s41467-020-19729-2.

(8) Marcandalli, G.; Monteiro, M. C. O.; Goyal, A.; Koper, M. T. M. Electrolyte Effects on CO2 Electrochemical Reduction to CO. *Acc. Chem. Res.* **2022**, *55* (14), 1900–1911. https://doi.org/10.1021/acs.accounts.2c00080.

(9) Ringe, S.; Clark, E. L.; Resasco, J.; Walton, A.; Seger, B.; Bell, A. T.; Chan, K. Understanding Cation Effects in Electrochemical CO2 Reduction. *Energy Environ. Sci.* **2019**, *12* (10), 3001–3014. https://doi.org/10.1039/c9ee01341e.

(10) Ren, Y.; Yu, C.; Tan, X.; Huang, H.; Wei, Q.; Qiu, J. Strategies to Suppress Hydrogen Evolution for Highly Selective Electrocatalytic Nitrogen Reduction: Challenges and Perspectives. *Energy Environ. Sci.* **2021**, *14* (3), 1176–1193. https://doi.org/10.1039/d0ee03596c.

(11) Westhead, O.; Spry, M.; Bagger, A.; Shen, Z.; Yadegari, H.; Favero, S.; Tort, R.; Titirici, M.; Ryan, M. P.; Jervis, R.; Katayama, Y.; Aguadero, A.; Regoutz, A.; Grimaud, A.; Stephens, I. E. L. The Role of Ion Solvation in Lithium Mediated Nitrogen Reduction. *J. Mater. Chem. A* **2022**, *11* (24), 12746–12758. https://doi.org/10.1039/d2ta07686a.

(12) Blanco, D. E.; Atwi, R.; Sethuraman, S.; Lasri, A.; Morales, J.; Rajput, N. N.; Modestino, M. A. Effect of Electrolyte Cations on Organic Electrosynthesis: The Case of Adiponitrile Electrochemical Production. *J. Electrochem. Soc.* **2020**, *167* (15), 155526. https://doi.org/10.1149/1945-7111/abc766.

(13) Baizer, M. M. Electrolytic Reductive Coupling: I. Acrylonitrile. *J. Electrochem. Soc.* **1964**, *111* (2), 215–222. https://doi.org/10.1149/1.2426088.

(14) Corbin, N.; Junor, G. P.; Ton, T. N.; Baker, R. J.; Manthiram, K. Toward Improving the Selectivity of Organic Halide Electrocarboxylation with Mechanistically Informed Solvent Selection. *J. Am. Chem. Soc.* **2023**, *145* (3), 1740–1748.

https://doi.org/10.1021/jacs.2c10561.

(15) Ishii, H.; Yamada, N.; Fuchigami, T. Electrolytic Partial Fluorination of Organic Compound. Part: 53 Highly Regioselective Anodic Mono- and Difluorination of 4-Arylthio-1,3-Dioxolan-2-Ones. A Marked Solvent Effect on Fluorinated Product Selectivity. *Tetrahedron* **2001**, *57* (44), 9067–9072. https://doi.org/10.1016/S0040-4020(01)00910-3.

(16) Dorchies, F.; Serva, A.; Crevel, D.; De Freitas, J.; Kostopoulos, N.; Robert, M.; Sel, O.; Salanne, M.; Grimaud, A. Controlling the Hydrophilicity of the Electrochemical Interface to Modulate the Oxygen-Atom Transfer in Electrocatalytic Epoxidation Reactions. *J. Am. Chem. Soc.* **2022**, *144* (49), 22734–22746. https://doi.org/10.1021/jacs.2c10764.

(17) Jin, K.; Maalouf, J. H.; Lazouski, N.; Corbin, N.; Yang, D.; Manthiram, K. Epoxidation of Cyclooctene Using Water as the Oxygen Atom Source at Manganese Oxide Electrocatalysts. *J. Am. Chem. Soc.* **2019**, *141* (15), 6413–6418. https://doi.org/10.1021/jacs.9b02345.

(18) Chung, M.; Jin, K.; Zeng, J. S.; Ton, T. N.; Manthiram, K. Tuning Single-Atom Dopants on Manganese Oxide for Selective Electrocatalytic Cyclooctene Epoxidation. *J. Am. Chem. Soc.* **2022**, *144* (38), 17416–17422. https://doi.org/10.1021/jacs.2c04711.

(19) Sun, Y.; Li, X.; Yang, M.; Xu, W.; Xie, J.; Ding, M. Highly Selective Electrocatalytic Oxidation of Benzyl C-H Using Water as Safe and Sustainable Oxygen Source. *Green Chem.* **2020**, *22* (21), 7543–7551. https://doi.org/10.1039/d0gc01871f.

(20) Park, J. K.; Lee, S. Sulfoxide and Sulfone Synthesis via Electrochemical Oxidation of Sulfides. *J. Org. Chem.* **2021**, *86* (19), 13790–13799. https://doi.org/10.1021/acs.joc.1c01657.

(21) Chung, M.; Maalouf, J. H.; Adams, J. S.; Jiang, C.; Román-Leshkov, Y.; Manthiram, K. Direct Propylene Epoxidation via Water Activation over Pd-Pt Electrocatalysts. *Science* **2024**, *383* (6678), 49–55. https://doi.org/10.1126/science.adh4355.

(22) Maalouf, J. H.; Jin, K.; Yang, D.; Limaye, A. M.; Manthiram, K. Kinetic Analysis of Electrochemical Lactonization of Ketones Using Water as the Oxygen Atom Source. *ACS*

Catal. **2020**, *10* (10), 5750–5756. https://doi.org/10.1021/acscatal.0c00931.

(23) Liu, C.; Chen, F.; Zhao, B.; Wu, Y.; Zhang, B. Electrochemical Hydrogenation and Oxidation of Organic Species Involving Water. *Nat. Rev. Chem.* **2024**, *8* (4), 277–293. https://doi.org/10.1038/s41570-024-00589-z.

(24) Amri, N.; Wirth, T. Flow Electrosynthesis of Sulfoxides, Sulfones, and Sulfoximines without Supporting Electrolytes. *J. Org. Chem.* **2021**, *86* (22), 15961–15972. https://doi.org/10.1021/acs.joc.1c00860.

(25) Li, P.; Guo, C.; Wang, S.; Ma, D.; Feng, T.; Wang, Y.; Qiu, Y. Facile and General Electrochemical Deuteration of Unactivated Alkyl Halides. *Nat. Commun.* **2022**, *13* (1), 3774. https://doi.org/10.1038/s41467-022-31435-9.

(26) Norcott, P. L. Current Electrochemical Approaches to Selective Deuteration. *Chem. Commun.* **2022**, *58* (18), 2944–2953. https://doi.org/10.1039/d2cc00344a.

(27) Wood, D.; Lin, S. Deuterodehalogenation Under Net Reductive or Redox-Neutral Conditions Enabled by Paired Electrolysis. *Angew. Chemie Int. Ed.* **2023**, *62*, e202218858. https://doi.org/10.1002/anie.202218858.

(28) Koverga, V.; Juhász, Á.; Dudariev, D.; Lebedev, M.; Idrissi, A.; Jedlovszky, P. Local Structure of DMF-Water Mixtures, as Seen from Computer Simulations and Voronoi Analysis. *J. Phys. Chem. B* **2022**, *126* (36), 6964–6978. https://doi.org/10.1021/acs.jpcb.2c02235.

(29) Liu, X.; Wang, S.; Xu, X.; Khair, H.; Dong, Z.; Wang, H.; Zhang, W.; Yu, T.; Men, Z.; Sun, C.; Wang, S. Exploring the Dynamic Changes in Hydrogen Bond Structure of Water and Heavy Water under External Perturbation of DMF. *Spectrochim. Acta - Part A Mol. Biomol. Spectrosc.* **2024**, *305*, 123493. https://doi.org/10.1016/j.saa.2023.123493.

(30) Tomar, D.; Rana, B.; Jena, K. C. The Structure of Water–DMF Binary Mixtures Probed by Linear and Nonlinear Vibrational Spectroscopy. *J. Chem. Phys.* **2020**, *152*, 114707. https://doi.org/10.1063/1.5141757.

(31) Venkataramanan, N. S. Cooperativity of Intermolecular Hydrogen Bonds in Microsolvated DMSO and DMF Clusters: A DFT, AIM, and NCI Analysis. *J. Mol.*

Model. **2016**, *22*, 151. https://doi.org/10.1007/s00894-016-3022-0.

(32) Dubouis, N.; Serva, A.; Berthin, R.; Jeanmairet, G.; Porcheron, B.; Salager, E.; Salanne, M.; Grimaud, A. Tuning Water Reduction through Controlled Nanoconfinement within an Organic Liquid Matrix. *Nat. Catal.* **2020**, *3* (8), 656–663. https://doi.org/10.1038/s41929-020-0482-5.

(33) Huang, N.; Nordlund, D.; Huang, C.; Bergmann, U.; Weiss, T. M.; Pettersson, L. G. M.; Nilsson, A. X-Ray Raman Scattering Provides Evidence for Interfacial Acetonitrile-Water Dipole Interactions in Aqueous Solutions. *J. Chem. Phys.* **2011**, *135* (16), 1–7. https://doi.org/10.1063/1.3655468.

(34) Takamuku, T.; Noguchi, Y.; Matsugami, M.; Iwase, H.; Otomo, T.; Nagao, M. Heterogeneity of Acetonitrile-Water Mixtures in the Temperature Range 279-307 K Studied by Small-Angle Neutron Scattering Technique. *J. Mol. Liq.* **2007**, *136* (1–2), 147–155. https://doi.org/10.1016/j.molliq.2007.02.009.

(35) Takamuku, T.; Tabata, M.; Yamaguchi, A.; Nishimoto, J.; Kumamoto, M.; Wakita, H.; Yamaguchi, T. Liquid Structure of Acetonitrile−Water Mixtures by X-Ray Diffraction and Infrared Spectroscopy. *J. Phys. Chem. B* **1998**, *102* (44), 8880–8888. https://doi.org/10.1021/jp9824297.

(36) Marcus, Y. The Structure of and Interactions in Binary Acetonitrile + Water Mixtures. *J. Phys. Org. Chem.* **2012**, *25* (12), 1072–1085. https://doi.org/10.1002/poc.3056.

(37) Liu, X.; Lee, S. C.; Seifert, S.; Winans, R. E.; Zhang, Y.; Li, T. Relationship of the Molecular Structure and Transport Properties of Imide-Based Lithium Salts of "Acetonitrile/Water-in-Salt" Electrolytes. *Chem. Mater.* **2023**, *35* (16), 6415–6422. https://doi.org/10.1021/acs.chemmater.3c01148.

(38) Dubouis, N.; Serva, A.; Salager, E.; Deschamps, M.; Salanne, M.; Grimaud, A. The Fate of Water at the Electrochemical Interfaces: Electrochemical Behavior of Free Water Versus Coordinating Water. *J. Phys. Chem. Lett.* **2018**, *9* (23), 6683–6688. https://doi.org/10.1021/acs.jpclett.8b03066.

(39) Venables, D. S.; Schmuttenmaer, C. A. Spectroscopy and Dynamics of Mixtures of Water

with Acetone, Acetonitrile, and Methanol. *J. Chem. Phys.* **2000**, *113* (24), 11222–11236. https://doi.org/10.1063/1.1328072.

(40) Perera, A.; Sokolić, F. Modeling Nonionic Aqueous Solutions: The Acetone-Water Mixture. *J. Chem. Phys.* **2004**, *121* (22), 11272–11282. https://doi.org/10.1063/1.1817970.

(41) Weerasinghe, S.; Smith, P. E. Kirkwood-Buff Derived Force Field for Mixtures of Acetone and Water. *J. Chem. Phys.* **2003**, *118* (23), 10663–10670. https://doi.org/10.1063/1.1574773.

(42) Takamuku, T.; Nakamizo, A.; Tabata, M.; Yoshida, K.; Yamaguchi, T.; Otomo, T. Large-Angle X-Ray Scattering, Small-Angle Neutron Scattering, and NMR Relaxation Studies on Mixing States of 1,4-Dioxane-Water, 1,3-Dioxane-Water, and Tetrahydrofuran-Water Mixtures. *J. Mol. Liq.* **2003**, *103–104* (Kolisch 1996), 143–159. https://doi.org/10.1016/S0167-7322(02)00133-2.

(43) McLain, S. E.; Soper, A. K.; Luzar, A. Investigations on the Structure of Dimethyl Sulfoxide and Acetone in Aqueous Solution. *J. Chem. Phys.* **2007**, *127* (17). https://doi.org/10.1063/1.2784555.

(44) Lotze, S.; Groot, C. C. M.; Vennehaug, C.; Bakker, H. J. Femtosecond Mid-Infrared Study of the Dynamics of Water Molecules in Water-Acetone and Water-Dimethyl Sulfoxide Mixtures. *J. Phys. Chem. B* **2015**, *119* (16), 5228–5239. https://doi.org/10.1021/jp512703w.

(45) Gupta, R.; Chandra, A. An Ab Initio Molecular Dynamics Study of Diffusion, Orientational Relaxation and Hydrogen Bond Dynamics in Acetone-Water Mixtures. *J. Mol. Liq.* **2012**, *165*, 1–6. https://doi.org/10.1016/j.molliq.2011.09.010.

(46) Freitas, L. C. G.; Cordeiro, J. M. M. Monte Carlo Simulation of Water-Tetrahydrofuran Mixtures. *J. Mol. Struct. THEOCHEM* **1995**, *335*, 189–195. https://doi.org/10.1016/0166-1280(94)04000-I.

(47) Korsunskii, V. I.; Naberukhin, Y. I. Microheterogeneous Structure of Aqueous Solutions of Nonelectrolytes X-Ray Diffraction Studies. *J. Struct. Chem.* **1977**, *18* (3), 470–482. https://doi.org/10.1007/BF00753094.

(48) Katayama, M.; Ozutsumi, K. The Number of Water-Water Hydrogen Bonds in Water-Tetrahydrofuran and Water-Acetone Binary Mixtures Determined by Means of X-Ray Scattering. *J. Solution Chem.* **2008**, *37* (6), 841–856. https://doi.org/10.1007/s10953-008-9276-0.

(49) Morcom, K. W.; Smith, R. W. Enthalpies of Mixing of Water+methyl Cyanide. *J. Chem. Thermodyn.* **1969**, *1* (5), 503–505. https://doi.org/10.1016/0021-9614(69)90009-3.

(50) Cilense, M.; Benedetti, A. V.; Vollet, D. R. Thermodynamic Properties of Liquid Mixtures. II. Dimethylformamide-Water. *Thermochim. Acta* **1983**, *63* (2), 151–156. https://doi.org/10.1016/0040-6031(83)80080-X.

(51) Benedetti, A. V.; Cilense, M.; Vollet, D. R.; Montone, R. C. Thermodynamic Properties of Liquid Mixtures. III. Acetone-Water. *Thermochim. Acta* **1983**, *66* (1–3), 219–223. https://doi.org/10.1016/0040-6031(93)85032-5.

(52) Inglese, A.; Ferino, I.; Marongiu, B.; Solinas, V.; Torrazza, S. Thermodynamic Properties of Aqueous Non-Electrolyte Mixtures. Excess Enthalpies of Water + Cyclic Ether Mixtures at 298.15 K. *Thermochim. Acta* **1983**, *65* (2–3), 169–177. https://doi.org/10.1016/0040-6031(83)80020-3.

(53) Susi, H. The Strength of Hydrogen Bonding: Infrared Spectroscopy. *Methods Enzymol.* **1972**, *26* (C), 381–391. https://doi.org/10.1016/S0076-6879(72)26019-0.

(54) Seki, T.; Chiang, K. Y.; Yu, C. C.; Yu, X.; Okuno, M.; Hunger, J.; Nagata, Y.; Bonn, M. The Bending Mode of Water: A Powerful Probe for Hydrogen Bond Structure of Aqueous Systems. *J. Phys. Chem. Lett.* **2020**, *11* (19), 8459–8469. https://doi.org/10.1021/acs.jpclett.0c01259.

(55) Dingley, A. J.; Cordier, F.; Grzesiek, S. An Introduction to Hydrogen Bond Scalar Couplings. *Concepts Magn. Reson.* **2001**, *13* (2), 103–127. https://doi.org/10.1002/1099-0534(2001)13:2<103::aid-cmr1001>3.3.co;2-d.

(56) Liu, X.; Fang, L.; Lyu, X.; Winans, R. E.; Li, T. Unveiling the Liquid Electrolyte Solvation Structure by Small Angle X-Ray Scattering. *Chem. Mater.* **2023**, *35* (23), 9821–9832. https://doi.org/10.1021/acs.chemmater.3c01648.

(57) Zoranić, L.; Mazighi, R.; Sokolić, F.; Perera, A. Concentration Fluctuations and Microheterogeneity in Aqueous Amide Mixtures. *J. Chem. Phys.* **2009**, *130*, 124315. https://doi.org/10.1063/1.3093071.

(58) Zoranić, L.; Mazighi, R.; Sokolić, F.; Perera, A. On the Microheterogeneity in Neat and Aqueous Amides: A Molecular Dynamics Study. *J. Phys. Chem. C* **2007**, *111* (43), 15586–15595. https://doi.org/10.1021/jp0736894.

(59) Biliškov, N.; Baranović, G. Infrared Spectroscopy of Liquid Water-N,N-Dimethylformamide Mixtures. *J. Mol. Liq.* **2009**, *144* (3), 155–162. https://doi.org/10.1016/j.molliq.2008.11.004.

(60) Bai, Y.; Zhou, D.; Mukherjee, S.; Liu, J.; Bian, H.; Fang, Y. Distinct Hydrogen Bonding Dynamics Underlies the Microheterogeneity in DMF-Water Mixtures. *J. Phys. Chem. B* **2022**, *126* (46), 9663–9672. https://doi.org/10.1021/acs.jpcb.2c06335.

(61) Jeffries, C. M.; Ilavsky, J.; Martel, A.; Hinrichs, S.; Meyer, A.; Pedersen, J. S.; Sokolova, A. V.; Svergun, D. I. Small-Angle X-Ray and Neutron Scattering. *Nat. Rev. Methods Prim.* **2021**, *1* (1), 70. https://doi.org/10.1038/s43586-021-00064-9.

(62) *Neutron activation and scattering calculator*. https://www.ncnr.nist.gov/resources/activation/ (accessed: 02-08-2024).

(63) Brehm, M.; Kirchner, B. TRAVIS - A Free Analyzer and Visualizer for Monte Carlo and Molecular Dynamics Trajectories. *J. Chem. Inf. Model.* **2011**, *51* (8), 2007–2023. https://doi.org/10.1021/ci200217w.

(64) Brehm, M.; Thomas, M.; Gehrke, S.; Kirchner, B. TRAVIS—A Free Analyzer for Trajectories from Molecular Simulation. *J. Chem. Phys.* **2020**, *152*, 164105. https://doi.org/10.1063/5.0005078.

(65) Ruiz, J.; Astruc, D. Permethylated Electron-Reservoir Sandwich Complexes as References for the Determination of Redox Potentials. Suggestion of a New Redox Scale. *Comptes Rendus l'Académie des Sci. - Ser. IIC - Chem.* **1998**, *1* (1), 21–27. https://doi.org/10.1016/s1251-8069(97)86255-0.

(66) Noviandri, I.; Brown, K. N.; Fleming, D. S.; Gulyas, P. T.; Lay, P. A.; Masters, A. F.;

Phillips, L. The Decamethylferrocenium/Decamethylferrocene Redox Couple: A Superior Redox Standard to the Ferrocenium/Ferrocene Redox Couple for Studying Solvent Effects on the Thermodynamics of Electron Transfer. *J. Phys. Chem. B* **1999**, *103* (32), 6713–6722. https://doi.org/10.1021/jp991381+.

(67) Aranzaes, J. R.; Daniel, M. C.; Astruc, D. Metallocenes as References for the Determination of Redox Potentials by Cyclic Voltammetry - Permethylated Iron and Cobalt Sandwich Complexes, Inhibition by Polyamine Dendrimers, and the Role of Hydroxy-Containing Ferrocenes. *Can. J. Chem.* **2006**, *84* (2), 288–299. https://doi.org/10.1139/V05-262.

(68) Hupp, J. T. The Ferrocene Assumption in Redox Thermodynamics: Implications from Optical Intervalence Studies of Ion Pairing to Ferrocenium. *Inorg. Chem.* **1990**, *29* (24), 5010–5012. https://doi.org/10.1021/ic00349a038.

(69) Zhao, Y.; Hu, X.; Stucky, G. D.; Boettcher, S. W. Thermodynamic, Kinetic, and Transport Contributions to Hydrogen Evolution Activity and Electrolyte-Stability Windows for Water-in-Salt Electrolytes. *J. Am. Chem. Soc.* **2024**, *146* (5), 3438–3448. https://doi.org/10.1021/jacs.3c12980.

(70) Wong, D. B.; Sokolowsky, K. P.; El-Barghouthi, M. I.; Fenn, E. E.; Giammanco, C. H.; Sturlaugson, A. L.; Fayer, M. D. Water Dynamics in Water/DMSO Binary Mixtures. *J. Phys. Chem. B* **2012**, *116* (18), 5479–5490. https://doi.org/10.1021/jp301967e.

(71) Idrissi, A.; Marekha, B.; Barj, M.; Jedlovszky, P. Thermodynamics of Mixing Water with Dimethyl Sulfoxide, as Seen from Computer Simulations. *J. Phys. Chem. B* **2014**, *118* (29), 8724–8733. https://doi.org/10.1021/jp503352f.

(72) Soper, A. K.; Luzar, A. Orientation of Water Molecules around Small Polar and Nonpolar Groups in Solution: A Neutron Diffraction and Computer Simulation Study. *J. Phys. Chem.* **1996**, *100* (4), 1357–1367. https://doi.org/10.1021/jp951783r.

(73) Tuckerman, M. E.; Marx, D.; Parrinello, M. The Nature and Transport Mechanism of Hydrated Hydroxide Ions in Aqueous Solution. *Nature* **2002**, *417* (6892), 925–929. https://doi.org/10.1038/nature00797.

(74) Marx, D.; Tuckerman, M. E.; Hutter, J.; Parrinello, M. The Nature of the Hydrated Excess Proton in Water. *Nature* **1999**, *397* (6720), 601–604. https://doi.org/10.1038/17579.

(75) Geissler, P. L.; Dellago, C.; Chandler, D.; Hutter, J.; Parrinello, M. Autoionization in Liquid Water. *Science* **2001**, *291* (5511), 2121–2124. https://doi.org/10.1126/science.1056991.

(76) Filhol, J. S.; Neurock, M. Elucidation of the Electrochemical Activation of Water over Pd by First Principles. *Angew. Chemie - Int. Ed.* **2006**, *45* (3), 402–406. https://doi.org/10.1002/anie.200502540.

(77) Andrieux, C. P.; Le Gorande, A.; Saveant, J. M. Electron Transfer and Bond Breaking. Examples of Passage from a Sequential to a Concerted Mechanism in the Electrochemical Reductive Cleavage of Arylmethyl Halides. *J. Am. Chem. Soc.* **1992**, *114* (17), 6892–6904. https://doi.org/10.1021/ja00043a039.

(78) Sim, B. A.; Milne, P. H.; Griller, D.; Wayner, D. D. M. Thermodynamic Significance of P+ and ρ- from Substituent Effects on the Redox Potentials of Arylmethyl Radicals. *J. Am. Chem. Soc.* **1990**, *112* (18), 6635–6638. https://doi.org/10.1021/ja00174a027.

(79) Bard, A. J.; Faulkner, L. R. *Electrochemical Methods: Fundamentals and Applications*, 2nd ed.; Wiley, 2001.

(80) Abraham, M. J.; Murtola, T.; Schulz, R.; Páll, S.; Smith, J. C.; Hess, B.; Lindahl, E. GROMACS: High Performance Molecular Simulations through Multi-Level Parallelism from Laptops to Supercomputers. *SoftwareX* **2015**, *1–2*, 19–25. https://doi.org/10.1016/j.softx.2015.06.001.

(81) Nosé, S. A Unified Formulation of the Constant Temperature Molecular Dynamics Methods. *J. Chem. Phys.* **1984**, *81* (1), 511–519. https://doi.org/10.1063/1.447334.

(82) Evans, D. J.; Holian, B. L. The Nose-Hoover Thermostat. *J. Chem. Phys.* **1985**, *83* (8), 4069–4074. https://doi.org/10.1063/1.449071.

(83) Martínez, L.; Andrade, R.; Birgin, E. G.; Martínez, J. M. PACKMOL: A Package for Building Initial Configurations for Molecular Dynamics Simulations. *J. Comput. Chem.* **2009**, *30* (13), 2157–2164. https://doi.org/10.1002/jcc.21224.

(84) Brehm, M.; Weber, H.; Thomas, M.; Hollóczki, O.; Kirchner, B. Domain Analysis in Nanostructured Liquids: A Post-Molecular Dynamics Study at the Example of Ionic Liquids. *ChemPhysChem* **2015**, *16* (15), 3271–3277. https://doi.org/10.1002/cphc.201500471.

(85) Cromer, D. T.; Mann, J. B. X-Ray Scattering Factors Computed from Numerical Hartree–Fock Wave Functions. *Acta Crystallogr. Sect. A* **1968**, *24* (2), 321–324. https://doi.org/10.1107/S0567739468000550.

(86) Humphrey, W.; Dalke, A.; Schulten, K. VMD: Visual Molecular Dynamics. *J. Mol. Graph.* **1996**, *14* (1), 33–38. https://doi.org/10.1016/0263-7855(96)00018-5.

TABLE OF CONTENTS GRAPHIC